

Enormous thermoelectric power factor of ZrTe₂/SrTiO₃ heterostructure

Chun Hung Suen

Hong Kong Polytechnic University

Songhua Cai

Nanjing University

Hui Li

The Hong Kong University of Science and Technology

Xiaodan Tang

College of Physics, Chongqing University

Huichao Wang

Peking University

Mingquan He

College of Physics, Chongqing University

Yisheng Chai

Chongqing University <https://orcid.org/0000-0003-0034-7488>

Kai Zhou

College of Physics, Chongqing University

Chi Man Wong

The Hong Kong Polytechnic University

Jiannong Wang

Hong Kong University of Science and Technology <https://orcid.org/0000-0002-6133-6371>

Xiaoyuan Zhou

Chongqing University

Jiyan Dai (✉ jiyan.dai@polyu.edu.hk)

Hong Kong Polytechnic University

Article

Keywords: Thermoelectric, ZrTe₂ thin film, high mobility, interface, transition metal dichalcogenides

Posted Date: January 12th, 2021

DOI: <https://doi.org/10.21203/rs.3.rs-89694/v1>

License: © ⓘ This work is licensed under a Creative Commons Attribution 4.0 International License.

[Read Full License](#)

Enormous thermoelectric power factor of ZrTe₂/SrTiO₃ heterostructure

Chun Hung Suen¹⁺, S.H. Cai¹⁺, Hui Li²⁺, Xiaodan Tang³, Huichao Wang^{4,*}, M.Q. He³, Y.S. Chai³, K. Zhou³, Chi Man Wong¹, Jiannong Wang,^{2,*} X. Y. Zhou^{3,*} and Ji-Yan Dai^{1,*}

¹ Department of Applied Physics, The Hong Kong Polytechnic University, Hung Hom, Kowloon, Hong Kong, China

² Department of Physics, Hong Kong University of Science and Technology, Clear Water Bay, Hong Kong, China

³ College of Physics, Chongqing University, Chongqing 401331, China

⁴ School of Physics, Sun Yat-sen University, Guangzhou 510275, China

Abstract

Achieving high thermoelectric power factor in thin film heterostructures is essential for integrated and miniaturized thermoelectric device applications. In this work, we demonstrate a mechanism to enhance thermoelectric power factor through coupling the interfacial confined two-dimensional electron gas (2DEG) with thin film conductivity in a transition metal dichalcogenides-SrTiO₃ heterostructure. Owing to the formed conductive interface with two-dimensional electron confinement effect and the elevated conductivity, the ZrTe₂/SrTiO₃ (STO) heterostructure presents enormous thermoelectric power factor as high as $4 \times 10^5 \mu W cm^{-1} K^{-2}$ at 20 K and $4800 \mu W cm^{-1} K^{-2}$ at room temperature. Interfacial reaction induced degradation of Ti cations valence number from Ti⁴⁺ to Ti³⁺ is attributed to be responsible for the formation of the quasi-two-dimensional electrons at the interface which results in very large Seebeck coefficient; and the enhanced electrical conductivity is suggested to be originated from the charge transfer induced doping in the ZrTe₂. By taking the thermal conductivity of STO substrate as a reference, the effective zT value of this heterostructure can reach 15 at 300 K. This superior thermoelectric property makes this heterostructure a promising candidate for future thermoelectric device, and more importantly, paves a new pathway to design promising high-performance thermoelectric systems.

Keywords: Thermoelectric; ZrTe₂ thin film; high mobility; interface; transition metal dichalcogenides

⁺ These authors contribute equally

^{*}corresponding contact:

Jiyan.dai@polyu.edu.hk; xiaoyuan2013@cqu.edu.cn; wanghch26@mail.sysu.edu.cn; phjwang@ust.hk

Introduction

Seeking high performance thermoelectric thin films is a hot topic in condensed matter physics and materials science and is attracting growing interests recently¹⁻⁶. The development of micro-cooling devices and miniaturized self-powered devices is technically important for improvement of large-scale integrated circuits, which drives the study of thermoelectric thin films. For example, in microprocessors, the “hot spot” regions with higher power density frequently cause the fatal thermal failure, and thin film-based thermoelectric device can be a potential solution for in-demand cooling of circuits. Furthermore, high-performance thermoelectric thin films are also essential to build micro-power generators for self-powered devices in environments where a thermal gradient exists; this is significant for power engineering and management in future electronics.

The performance of a thermoelectric material can be evaluated by a dimensionless figure of merit $zT = S^2\sigma T/(\kappa_e + \kappa_l)$, where S , σ , T , κ_e , and κ_l represent Seebeck coefficient, electrical conductivity, absolute temperature, electronic thermal conductivity and lattice thermal conductivity, respectively^{7,8}. To enhance the figure of merit, numerous efforts have been devoted to improve the power factor (power factor = $S^2\sigma$)⁹⁻¹³ or reduce the thermal conductivity¹⁴⁻¹⁸. Among those methods to realize large thermoelectric power factor in a thin film/substrate heterostructure, interface engineering has been proven to be an effective approach to enhance Seebeck effect of the heterostructure. Especially, the presence of quasi-two-dimensional electron gas (quasi-2DEGs) at the interface is a dominant factor to the enhancement of $|S|$ ^{1,19-22}. As an ideal substrate with unique physical and chemical properties, SrTiO₃ (STO) has been widely applied in thin film growth as well as the exploration of novel low-dimensional physics^{1,23-28}. For example, the unique electronic phenomena generated from the heterointerface between epitaxial oxide layer and the STO substrate such as the very intriguing LaAlO₃/SrTiO₃ system has raised much attention. However, although the LAO/STO interface generally shows enhanced $|S|$, itself has not been found to exhibit an outstanding thermoelectric power factor mainly due to the limitation of its low conductivity at room temperature. For designing a viable high-performance thermoelectric system, it is necessary to couple both high conductivity and the enhanced thermoelectricity on a single hetero-interface.

Here, we demonstrate the realization of giant thermoelectric power factor in ZrTe₂/SrTiO₃ heterostructure, which mainly attribute to the coupling between interfacial quasi-2DEG generated on STO surface and the high conductivity of transition metal dichalcogenides (TMDs) film. An interfacial reaction between the pulsed-laser deposition (PLD) grown layered ZrTe₂ thin film and STO substrate leads to the appearance of quasi-2DEG which results in a great enhancement of the Seebeck coefficient. Meanwhile, the conductivity is also dramatically enhanced which may result from the doping effect of TMD film induced by charge transfer from the interface. Combining both the high Seebeck coefficient and electrical conductivity, this heterostructure system eventually presents an outstanding thermal power factor as well as thermoelectric figure of merit zT value. This work provides a promising

pathway for designing of high-performance thermoelectric systems, and opens up new possibilities for exploration and development of intriguing thermoelectric materials, structures as well as thin film-based thermoelectric devices.

Methods

In this study, PLD was used to grow ZrTe₂ films using an alloy target with Zr:Te=1:5 on the (100) STO substrates. The substrate-target distance during the deposition was 5 cm, with the base pressure of around 5×10^{-5} Pa, and the films were grown at optimized substrate temperature (T_s) of 550 °C. To prevent the ZrTe₂ film from oxidation in air, an amorphous AlN capping layer of ~ 70 nm thick was deposited on top of the ZrTe₂ film at 200 °C. The laser source was a KrF excimer laser with a wavelength of 248 nm. ZrTe₂ films with different thicknesses from 5 nm to 10 nm, 35 nm and 60 nm were deposited on STO substrates.

X-ray Diffraction (XRD) with Cu $K\alpha_1$ source was used to determine the orientation and crystallinity of ZrTe₂ film. To determine the microstructure and thickness of ZrTe₂ film, transmission electron microscope (TEM) was used for cross-sectional characterization. High-resolution TEM (HRTEM) images were acquired on JEOL 2100F TEM, operated at 200 kV. Scanning TEM (STEM) images were acquired on Thermofisher Titan G2 60-300 aberration corrected S/TEM. The accelerating voltage of electron beam is 300 kV. The convergence angle of electron probe for STEM-HAADF imaging is 22.5 mrad and the collection angle of annular detector is 79.5-200 mrad. A Gatan dual-EELS system was used for STEM-EELS data acquisition. For EELS line scan, the acquisition time per pixel is 1 s. The acquisition energy range is 420 to 720 eV with 0.1 eV dispersion, including the major or minor edges of oxygen and Ti. A 16T-PPMS (Physical Properties Measurement System) was utilized to measure the Seebeck coefficient and electrical conductivity at a temperature range from 0.5 K to 300 K. The measurement of Seebeck coefficient and electrical conductivity in the range from 300 K to 600 K was carried out on Joule Yacht MRS-3 thin film thermoelectric parameter test system.

Results and discussion

The microstructure and composition of all samples were firstly investigated using various methods. Figure 1(a) shows the cross-sectional HRTEM image of a 35 nm-thick ZrTe₂ film grown on STO substrate with a AlN capping layer. As it can be seen, between the STO substrate and AlN capping layer most parts of film clearly show (0001) ZrTe₂ lattice fringes parallel or nearly parallel to the substrate. This result is consistent with the expected layered structure of ZrTe₂ as shown schematically in Figure 1(b). ZrTe₂ has a hexagonal close-packed crystal structure with space group of $P\bar{3}m1$, and its 1T structure has an octahedral coordination of metal atoms²⁹ that can be illustrated as a CdI₂-type structure³⁰. A unit cell of ZrTe₂ is denoted by a cyan rectangle in Figure 1(b) and can also be identified in the magnified HRTEM image. The crystal structure of our ZrTe₂ film was also characterized by XRD. Figure 1(c) presents the XRD pattern of the sample with 60 nm-thick film, where peaks at 2θ

= 13.3 °, 26.9 °, 40.8 ° and 55.4 ° correspond to the *c*-axis (0001), (0002), (0003) and (0004) diffraction peaks of hexagonal ZrTe₂ (*a* = 0.395 nm, *c* = 0.663 nm, JCPDS #54-560), respectively. These results imply that the ZrTe₂ film is preferentially grown along *c*-axis, which is consistent with the HRTEM observations. However, it should be pointed out that, besides the dominating *c*-axis orientation peaks, other orientation peaks are also found in XRD, suggesting that the growth of ZrTe₂ film on STO is non-epitaxial.

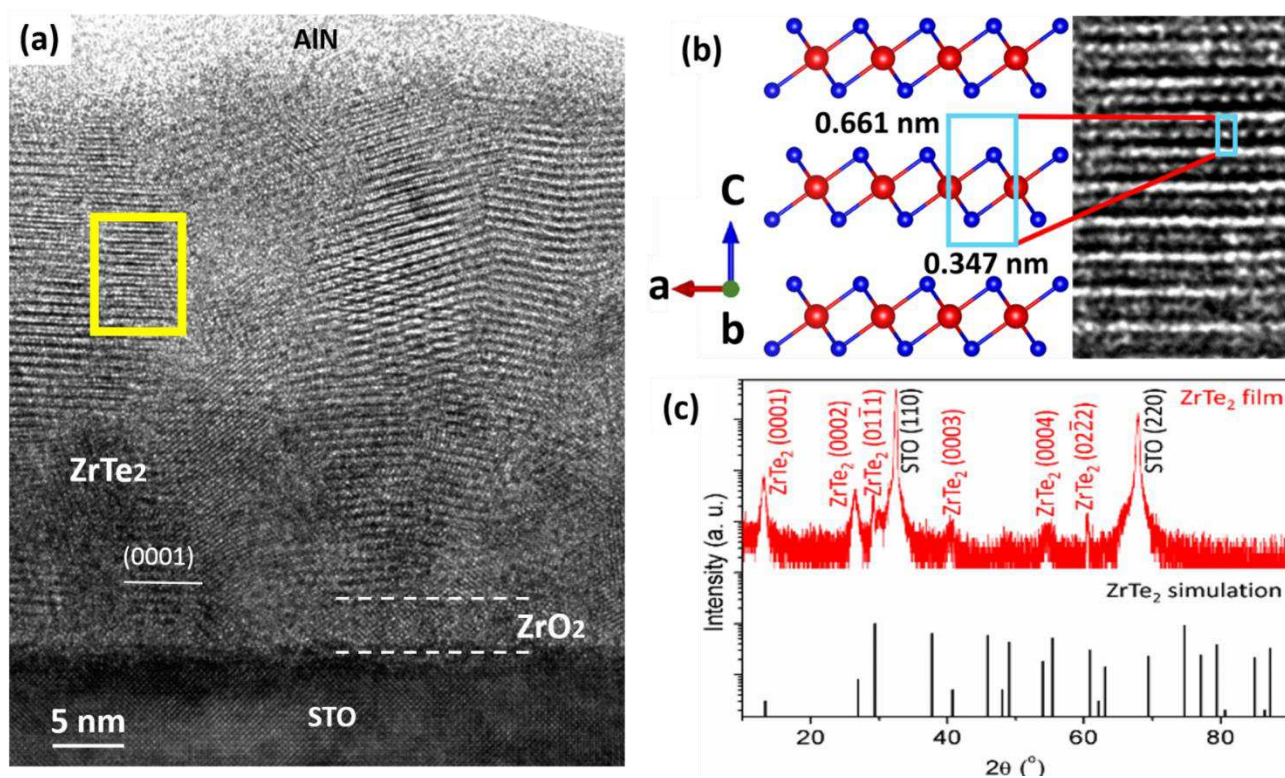


Figure 1 Crystal structure characterizations. (a) High-resolution TEM image of the ZrTe₂ film on STO substrate, where an interfacial layer of ZrO₂ reaction phase can be identified between the STO substrate and the ZrTe₂ film. (b) Magnified image of yellow rectangle region in (a) showing the correspondence of real unit cell with the crystal structure model of ZrTe₂. The unit cell is denoted by a rectangle to compared with magnified high-resolution TEM image of the ZrTe₂ film. (c) Typical XRD patterns of 60 nm ZrTe₂ film. The ZrTe₂ simulation pattern (JCPDS #54-560) is also illustrated for comparison.

It is worth noting that between the layered ZrTe₂ and the STO substrate, there exists a ~5 nm thick interfacial layer with a different lattice structure to ZrTe₂. A detailed analysis of the lattice spacings and their angles suggests that this interfacial layer is ZrO₂ (See Figure S1). This implies that interfacial reaction occurs between the deposited ZrTe₂ film and the STO substrate, and the interfacial characteristic has remarkably influenced the physical properties of both the ZrTe₂ film and the STO substrate. This can be revealed by the STEM energy disperse x-ray (EDX) spectroscopy element

mapping and the electron energy loss spectroscopy (EELS) analysis of the interfacial region as shown in Figure 2. A sample with relatively thin ZrTe₂ film (10 nm thick) was selected to reveal the overall elemental distribution of the whole sample. It is apparent in EDX mapping results shown in Figure 2(a), that the distributions of O and Te are not uniform along the thickness direction, i.e., the signal intensity of Te increases near the interface with a decrease of O signal. It is surprising to see that O even exists in the whole film, suggesting an out diffusion of O from STO which can be proven by EELS line-scan analysis across the interface as shown in Figure 2(b) and (c). By extracting the signals of Ti and O edges from the EELS spectrum, the energy loss near edge structures (ELNES) reveals that the 4 unit cells of STO from interface exhibits a different chemical state with bulk STO. From the 4th layer of STO up to the interfacial layer, the valence state of Ti cations degrades from Ti⁴⁺ to Ti³⁺ (peak shift and shape variation in Figure 2(b) with a corresponding change of O K-edge fine structure (Figure 2(c)). The interfacial characteristics imply a conductive STO surface, which is analogous to the similar situation in the oxide heterostructures such as LAO/STO.

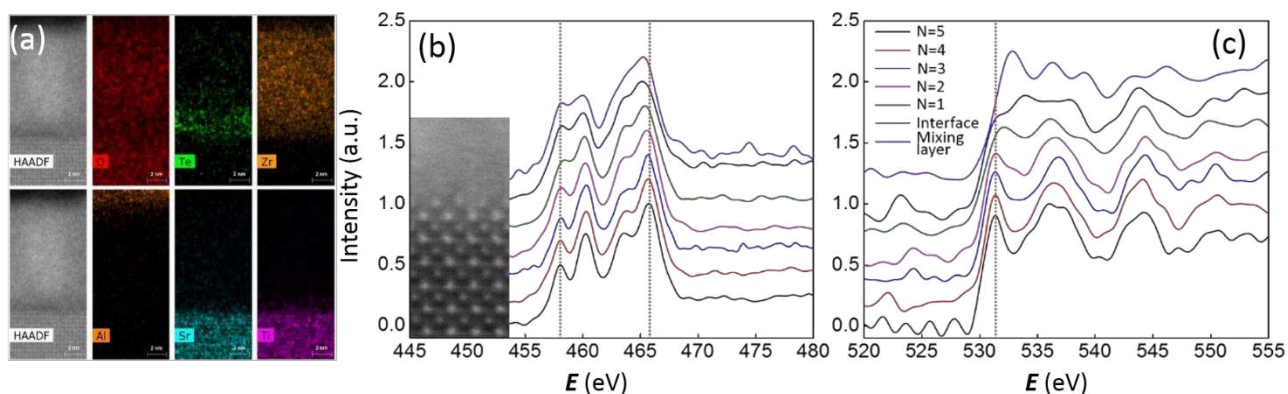


Figure 2 Elemental mapping and interfacial valence states of Ti and O ions. (a) STEM-EDS element mapping across the interface, (b) EELS results of Ti-3d L edge shift peaks, and (c) O-2p K edge fine structure across the interface.

We have carried out thermoelectric and electron transport properties measurements to different thicknesses of samples at temperatures ranging from 2 K to 600 K. The ZrTe₂/STO heterostructures exhibit negative Seebeck coefficient throughout the whole temperature range, indicating a n-type conducting characteristic; and the general trend is that the thicker films show relatively lower Seebeck coefficient but with high electrical conductivity, while very thin films present highly fluctuated Seebeck coefficient and high resistance. Figure 3(a) shows the temperature-dependent Seebeck coefficients of the ZrTe₂/STO heterostructures with 35 nm and 60 nm-thick ZrTe₂ films from 2 K to 600 K. The Seebeck coefficient in the sample with a 35 nm-thick ZrTe₂ generally increases with the temperature increases from 2 K and finally reaches the maximum value of about 530 μ V/K at 440 K, above which the Seebeck coefficient begins to decrease. The sample with 60 nm-thick ZrTe₂ film shows a similar trend while the maximum Seebeck coefficient appears at 111 K with a value of 368

$\mu\text{V}/\text{K}$. The temperature-dependent electrical conductivity of both samples are shown in Figure 3(b), which confirms that these heterostructures are highly conductive. The electrical conductivity can reach a remarkable value up to 10^7 S/cm at low temperature state (2 K). The coexistence of both very large Seebeck coefficient and very high electrical conductivity of the ZrTe_2/STO heterostructure consequently leads to enormous thermoelectric power factor. As shown in Figure 3(c), the thermoelectric power factors monotonically increase with the decreasing of temperature in both samples and finally achieve a colossal value even exceeds $3 \times 10^5 \mu\text{Wcm}^{-1}\text{K}^{-2}$ at 20 K.

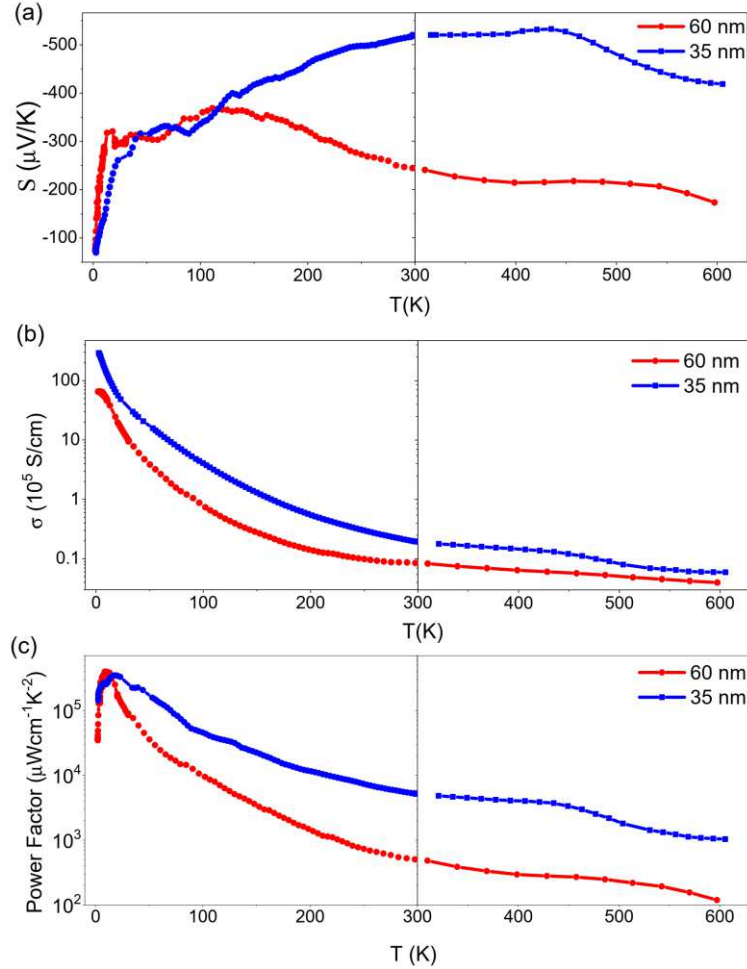


Figure 3 Thermoelectric and electrical conductive properties. (a) Seebeck coefficients, (b) electrical conductivities, and (c) thermoelectric power factors, of the ZrTe_2/STO heterostructures with 35 nm and 60 nm-thick ZrTe_2 films.

As well known, quasi-2DEG can exist in the conductive STO interface and its presence can be a prime factor for triggering intriguing thermoelectric properties. To clarify the contribution of the possible interfacial effect to the outstanding thermoelectric properties, we further conducted systematic electron transport measurements on the heterostructure. As a follow-up to our previous work²⁹, in these high quality heterostructures, we observed obvious Shubnikov–de Haas (SdH) oscillations superimposed

on the large magnetoresistance at low temperatures below 4 K. Figure 4(a) shows the oscillations after subtracting a smooth background from the measured magnetoresistance of a typical 60 nm-thick ZrTe₂ film on STO. The periodicity in the reciprocal of magnetic field ($1/B$) demonstrates that the SdH effect is the origin. Fast Fourier Transform (FFT) results further reveal that the oscillating frequency peak is about 29.5 T as shown in Figure 4(b). By analyzing the temperature dependence of the oscillations using the Lifshitz-Kosevitch formula, we obtain an effective mass of $1.3m_0$ where m_0 represents the rest mass of an electron (Figure 4(c)). In addition, the Dingle temperature is calculated as 1.4 K based on the measured quantum oscillations. It is interesting to find that the microscopic parameters of the quantum oscillations actually agree well with those acquired in conductive STO surfaces³¹⁻³⁸. Thus, we believe that the interfacial effect between the ZrTe₂ thin film and the STO substrate plays a significant role for presenting the very exotic transport properties in our observation²⁹.

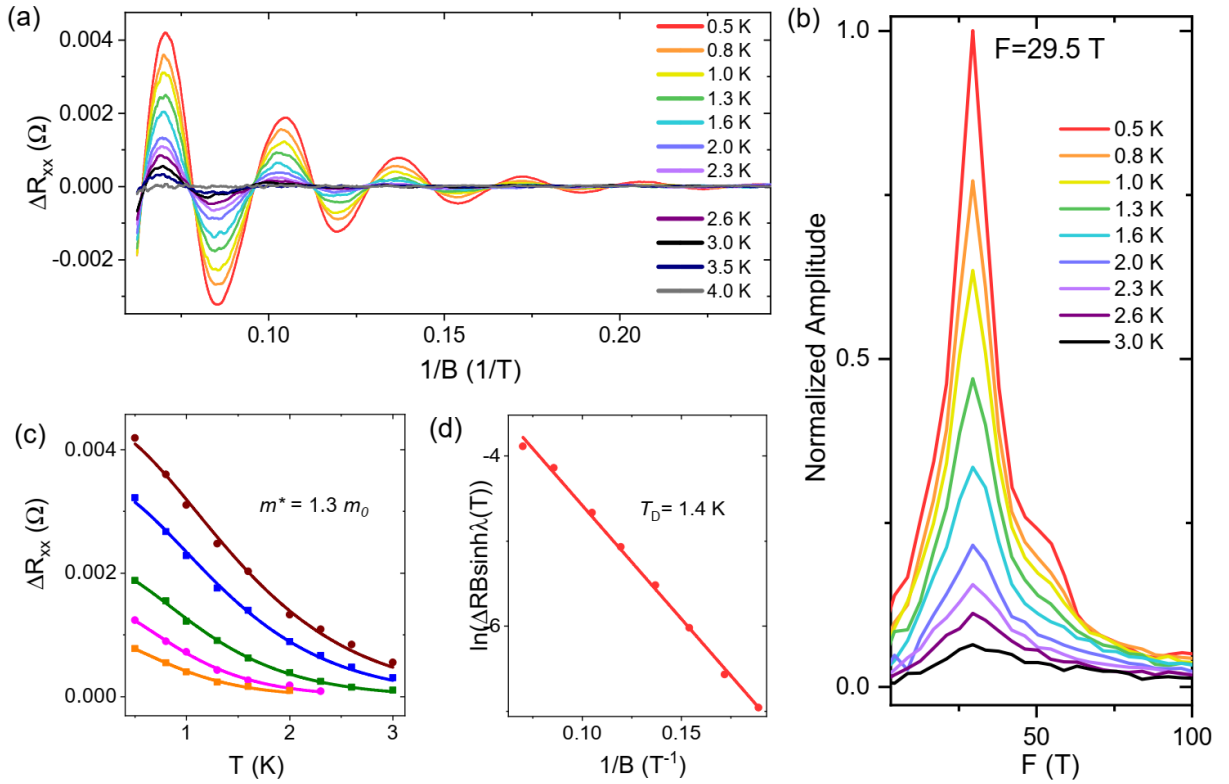


Figure 4 Quasi two-dimensional transport characteristics of the heterostructure. (a) SdH quantum oscillations in the ZrTe₂/STO, and (b) FFT results of the oscillations revealing a frequency peak of 29.5 T. (c) and (d) are calculated effective mass and Dingle temperature based on the Lifshitz-Kosevitch formula.

Our previous study on the ZrTe₂/STO heterostructures has revealed a quasi-2D transport characteristic of the hybrid heterostructure, within which the electrons exhibit a high mobility of about $1.8 \times 10^4 \text{ cm}^2 \text{ V}^{-1} \text{ s}^{-1}$ at 2 K²⁹. The quasi-2D transport feature is consistent to the layered structure

of ZrTe₂ and the property of quasi-2D electrons in the STO interface as well. These characteristics are supposed to be responsible for the observed enormous Seebeck coefficient and power factor. Similar findings also exist in TiO₂/STO, LAO/STO and FeSe/STO heterostructures^{1,39,40}. In the TiO₂/STO heterostructure, with the presence of 2DEG, the room temperature (300 K) Seebeck coefficient is as large as 1050 $\mu\text{V}/\text{K}$; while our ZrTe₂/STO heterostructures show a value of $|S|_{300\text{K}}$ smaller than 500 $\mu\text{V}/\text{K}$ (Figure 3(a)). It is worth noting that the Seebeck coefficient of the heterostructure shows obvious dependency with the thickness of the TMD film that a thicker ZrTe₂ film leads to the decrease of $|S|$. Figure S2 shows comparison of our results to reported Seebeck coefficients from other 2D systems. In fact, a control sample with only the ZrO₂/STO interfacial contribution shows much higher Seebeck coefficient with a value of about 750 $\mu\text{V}/\text{K}$ at 300 K, well consistent with the result in the TiO₂/STO heterostructure¹ (see Figure S3(b)). Meanwhile, the electrical conductivity is also found to be thickness dependent; while this dependence is opposite to that of the Seebeck coefficient. The control sample with only ZrO₂/STO shows a much higher resistance, making the Seebeck coefficient measurement fluctuate vigorously and also prevents the system achieving a higher power factor. As a conclusion, the deposition of TMD ZrTe₂ thin films on the top of the quasi-2D system results in slight decrease of the Seebeck coefficient of the system due to its relatively lower Seebeck coefficient, but it contributes very high conductivity to the system. With the coupling between the thin ZrTe₂ film and the STO-based interface, the largest thermoelectric power factor can be achieved in the ZrTe₂/STO heterostructure.

However, it should be noted that for a much thinner thickness, the interface is not well conductive and EELS results show that the valence state of Ti cations at the interfacial region is still Ti⁴⁺ instead of Ti³⁺ (see Figure S4). Therefore, we come to the conclusion that the interfacial state for forming a confined 2D conductive interface is essential for achieving the outstanding thermoelectric properties in this system. On the other hand, the extremely high conductivity is another crucial factor for realization of the giant thermopower factor. We also prepared a ZrTe₂ thin film on the insulating Al₂O₃ (Figure S5) to clarify the origin. It can be found that the ZrTe₂ thin film is indeed metallic with a high conductivity but still lower than the value achieved in the ZrTe₂/STO system; this also suggests a modulation effect to the ZrTe₂ film from the interface. As a reference, the FeSe/STO is a well-explored metal/STO heterostructure system due to the interface-enhanced high temperature superconductivity^{41,42}. Strong evidences have shown that the interfacial electron-phonon coupling as well as the electron doping on the FeSe layer should be responsible for the high temperature superconductivity of the FeSe/STO system⁴³⁻⁴⁷. In particular, the electron doping to the film through the thermal annealing generally decreases the resistance of the system and thus enhances the conductivity⁴⁸. We suggest that similar mechanism may also exist in the metallic ZrTe₂/STO heterostructure that the electron doping from the substrate to the TMD film determines the very high conductivity of the system. More efforts are needed to further demonstrate the underlying physical origins.

It is noticeable that there exists a small peak in the Seebeck coefficient at about 20 K (Figure 3(a)), and this can be explained by the phonon-drag effect⁴⁹⁻⁵¹ originated from the STO (100) substrate. One study that related to the thermal transport of STO⁵² exhibits a thermal conductivity peak close to 20 K. When a thermal gradient is applied to the thin film and substrate, nonequilibrium phonons will be generated and transfer their momentum to the carriers; as a result, an additional electric field is formed in the film, thus enhance the Seebeck coefficient. The characteristic of phonon-drag effect is that, it is more effective at temperatures where the substrate attains its maximum thermal conductivity; this is the reason why the peak of Seebeck coefficient, as shown in Figure 3(a), is near the temperature where the substrate exhibits its peak thermal conductivity.

For thin films, the substrate thermal conductivity dominated the thermal transport, so we estimate the effective thermoelectric figure of merit zT mainly based on the value of thermoelectric power factors of the film and the reported thermal conductivity values of STO single crystal⁵³. For the 35 nm ZrTe₂/STO sample, the effective zT value at 300 K is about 15, which is extremely higher compared to most of the reported works according to the best our knowledge^{3,54}. Even for the 60 nm thick ZrTe₂ film sample, the effective zT is about 1.5 at 300 K and increases to 13 at 18 K. This superior thermoelectric property makes this heterostructure a promising candidate for future thermoelectric device.

Conclusion

In summary, we demonstrate that the ZrTe₂/STO heterostructure possesses colossal thermoelectric power factor at both low temperature and room temperature. The excellent thermoelectric properties can be attributed to the formation of two-dimensional electrical transport property as well as the enhanced conductivity due to charge transfer occurs in the interface. This study reveals the promising thermoelectric properties of ZrTe₂/STO heterostructure and provides a new pathway for development of thermoelectric materials and structures. Furthermore, the mechanism exploration is of fundamental importance for both thermoelectric physics and possible application on thin film-based electronic devices.

Acknowledgements

We thank support from The Hong Kong Polytechnic University (Grant Nos. 1-ZVCG, 1-ZVGH, 4-ZZDC, and DD7F). X. Zhou acknowledges financial support from National Natural Science Foundation of China (NSFC) (Grant No. 11674040, 11904039) and the Fundamental Research Funds for the Central Universities (Grant no. 2018CDQYWL0048, 106112017CDJQJ308821 and 2018CDPTCG0001/26). H.W. acknowledges the support of the Hundreds of Talents program of Sun Yat-Sen University and the Fundamental Research Funds for the Central Universities (No. 201gpy165). H.Li and J.Wang acknowledge the financial support from the Research Council of the Hong Kong SAR (Grant Nos. 16307019, C7036-17W-1, and C6013-16E).

Supporting Information for

Enormous thermoelectric power factor of ZrTe₂/SrTiO₃ heterostructure

Chun Hung Suen¹⁺, S.H. Cai¹⁺, Hui Li,²⁺ Xiaodan Tang,³ Huichao Wang^{4}, M.Q. He³, Y.S. Chai³, K.*

Zhou³, Chi Man Wong¹, Jiannong Wang,^{2,} X. Y. Zhou^{3,*} and Ji-Yan Dai^{1,*}*

¹ Department of Applied Physics, The Hong Kong Polytechnic University, Hung Hom, Kowloon, Hong Kong, China

² Department of Physics, Hong Kong University of Science and Technology, Hong Kong, China

³ College of Physics, Chongqing University, Chongqing 401331, China

⁴ School of Physics, Sun Yat-sen University, Guangzhou 510275, China

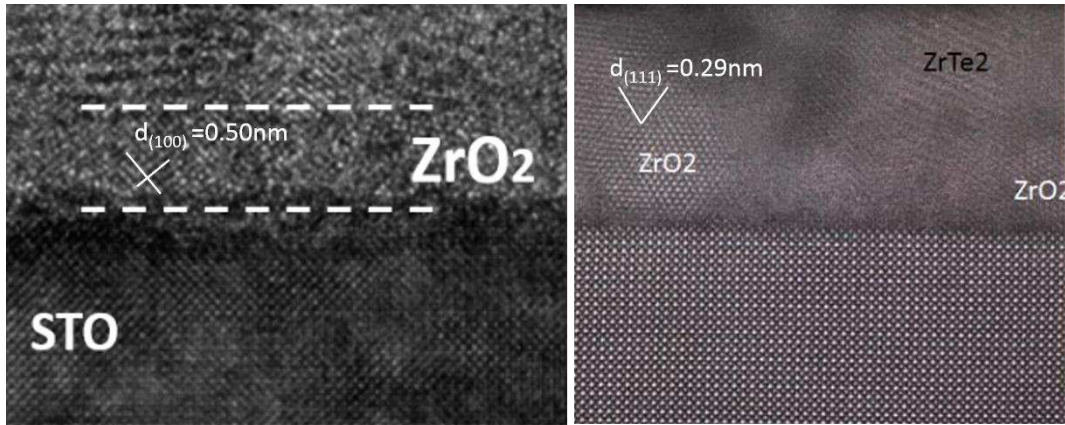


Figure S1 Detailed microstructure of the interface. (a) HRTEM, and (b) STEM, images of the interfacial structure. ZrO_2 becomes the dominant component near the interface area.

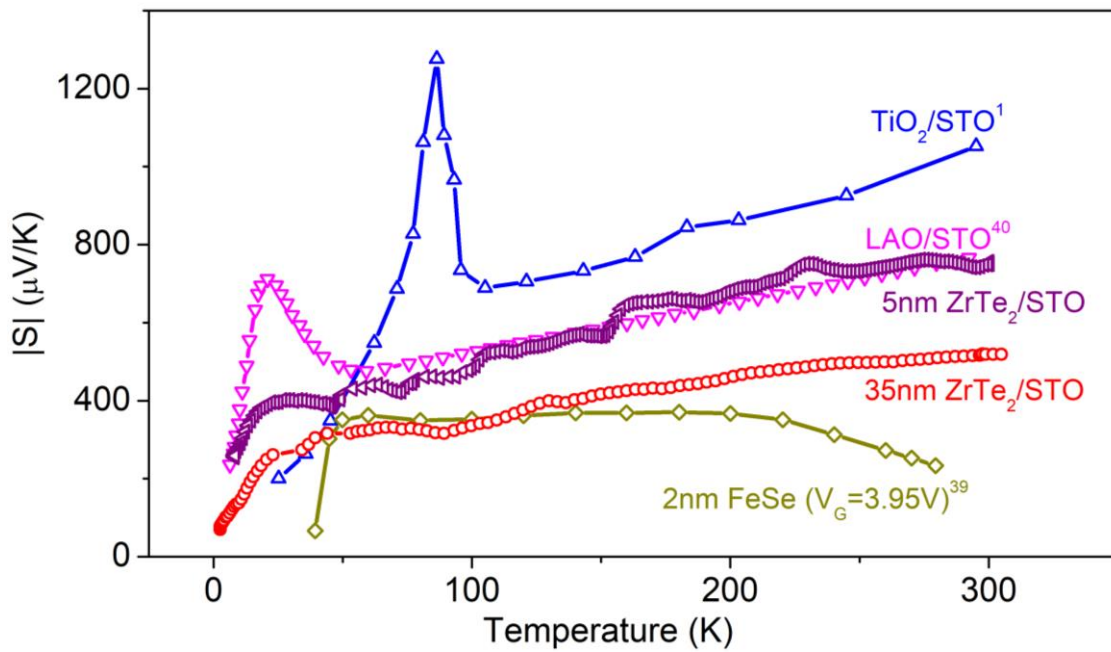


Figure S2 Comparison of temperature-dependent Seebeck coefficients with literatures among 2D systems.

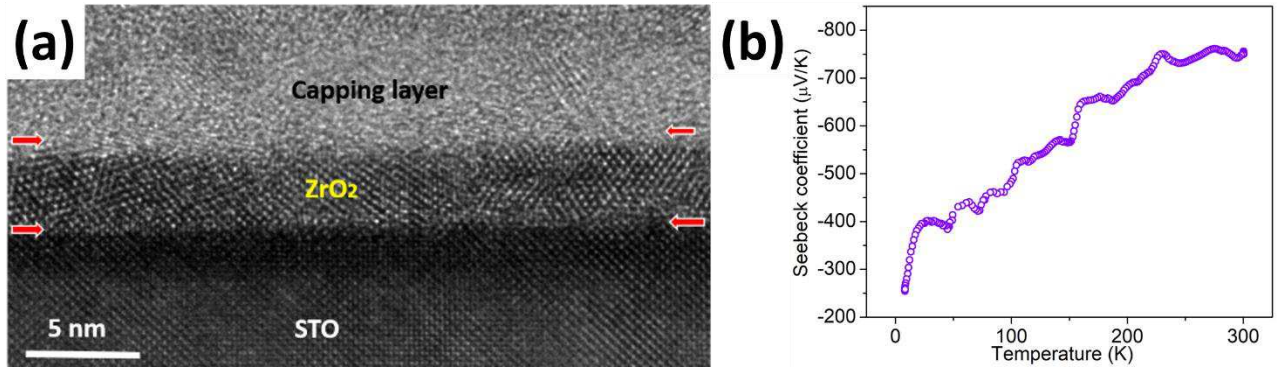


Figure S3 Microstructure and Seebeck coefficient of control sample (only 5nm-thick ZrO₂ film on STO). (a) HRTEM image, and (b) the Seebeck coefficient showing that the control sample has much larger Seebeck effect but unstable due to its high resistance. This ZrO₂/STO heterostructure was formed by PLD sputtering of Zr target at the same condition of ZrTe₂ film growth.

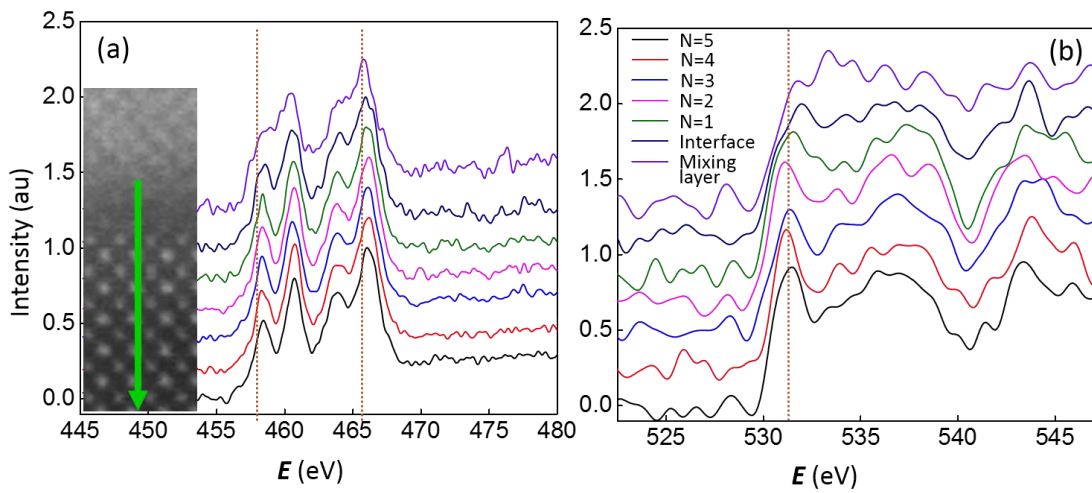


Figure S4 Interfacial valence states of Ti and O ions in thinnest control sample (5nm-thick ZrO₂ film on STO). (a) EELS results of Ti-3d L edge shift peaks, and (b) O-2p K edge fine structure across the interface.

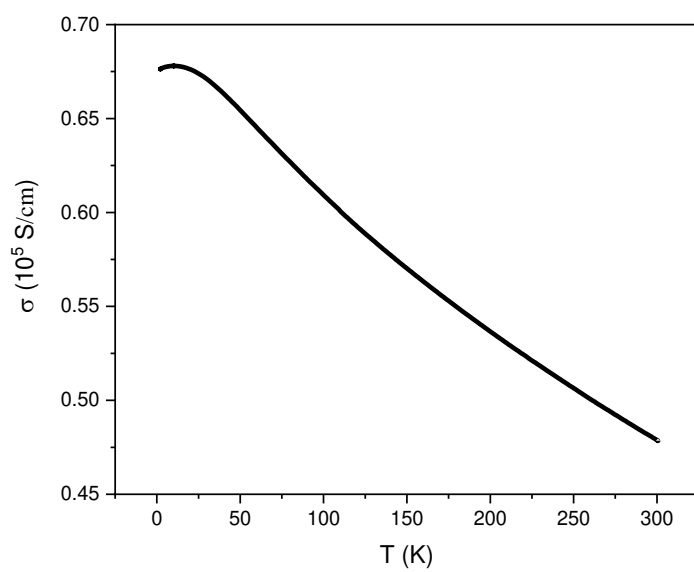


Figure S5 Conductivity-temperature relationship of the ZrTe_2 thin film on Al_2O_3 substrate.

References

- 1 Ohta, H. *et al.* Giant thermoelectric Seebeck coefficient of a two-dimensional electron gas in SrTiO₃. *Nat Mater* **6**, 129-134 (2007).
- 2 Rama, V., Edward, S., Thomas, C. & Brooks, O. Q. Thin-film thermoelectric devices with high room-temperature figures of merit. *Nature* **413**, 597-602 (2001).
- 3 Chen, X., Zhou, Z., Lin, Y.-H. & Nan, C. Thermoelectric thin films: Promising strategies and related mechanism on boosting energy conversion performance. *Journal of Materiomics* **6**, 494-512 (2020).
- 4 Shi, X.-L., Zou, J. & Chen, Z.-G. Advanced Thermoelectric Design: From Materials and Structures to Devices. *Chemical Reviews* **120**, 7399-7515 (2020).
- 5 Hong, S. *et al.* Wearable thermoelectrics for personalized thermoregulation. *Sci. Adv.* **5** (2019).
- 6 Kanahashi, K., Pu, J. & Takenobu, T. 2D Materials for Large-Area Flexible Thermoelectric Devices. *Advanced Energy Materials* **10** (2019).
- 7 Altenkirch, E. Über den Nutzeffekt der Thermoauale. *Physikalische Zeitschrift* **10** (1909).
- 8 Altenkirch, E. Electrothermische Kalteerzeugung and Reversible Electriche Heizung. *Physikalische Zeitschrift* **12**, 920 (1911).
- 9 Hicks, L. D. & Dresselhaus, M. S. Effect of quantum-well structures on the thermoelectric figure of merit. *Physical Review B* **47**, 12727-12731 (1993).
- 10 Heremans, J. P. *et al.* Enhancement of Thermoelectric Efficiency in PbTe by Distortion of the Electronic Density of States. *Science* **321**, 554-557 (2008).
- 11 Pei, Y. *et al.* Convergence of electronic bands for high performance bulk thermoelectrics. *Nature* **473**, 66-69 (2011).
- 12 Liu, W. *et al.* Convergence of conduction bands as a means of enhancing thermoelectric performance of n-type Mg₂Si_{1-x}Sn_x solid solutions. *Phys. Rev. Lett.* **108**, 166601 (2012).
- 13 Suen, C. H. *et al.* Enhanced thermoelectric properties of SnSe thin films grown by pulsed laser glancing-angle deposition. *Journal of Materiomics* **3**, 293-298 (2017).
- 14 Biswas, K. *et al.* High-performance bulk thermoelectrics with all-scale hierarchical architectures. *Nature* **489**, 414-418 (2012).
- 15 Hsu, K. F. *et al.* Cubic AgPb_mSbTe_{2+m}: Bulk Thermoelectric Materials with High Figure of Merit. *Science* **303**, 818-821 (2004).
- 16 Zhao, L.-D. *et al.* Ultralow thermal conductivity and high thermoelectric figure of merit in SnSe crystals. *Nature* **508**, 373-377 (2014).
- 17 Peng, K. *et al.* Broad temperature plateau for high ZTs in heavily doped p-type SnSe single crystals. *Energy & Environmental Science* **9**, 454-460 (2016).
- 18 Liu, H. *et al.* Copper ion liquid-like thermoelectrics. *Nat. Mater.* **11**, 422-425 (2012).
- 19 Nagase, K., Takado, S. & Nakahara, K. Thermoelectric enhancement in the two-dimensional

- electron gas of AlGaN/GaN heterostructures. *physica status solidi (a)* **213**, 1088-1092 (2016).
- 20 Ohta, H., Kim, S. W., Kaneki, S., Yamamoto, A. & Hashizume, T. High Thermoelectric Power Factor of High-Mobility 2D Electron Gas. *Adv Sci (Weinh)* **5**, 1700696 (2018).
- 21 Rhyee, J. S. *et al.* Peierls distortion as a route to high thermoelectric performance in In₄Se_{3-δ} crystals. *Nature* **459**, 965-968 (2009).
- 22 Fukutani, K., Sato, T., Galiy, P. V., Sugawara, K. & Takahashi, T. Tunable two-dimensional electron gas at the surface of thermoelectric material In₄Se₃. *Physical Review B* **93**, 205156 (2016).
- 23 Ohtomo, A. & Hwang, H. Y. A high-mobility electron gas at the LaAlO₃/SrTiO₃ heterointerface. *Nature* **427**, 423-426 (2004).
- 24 Reyren, N. *et al.* Superconducting Interfaces Between Insulating Oxides. *Science* **317**, 1196-1199 (2007).
- 25 Gabay, M. & Triscone, J.-M. Hund rules with a twist. *Nature Physics* **9**, 610-611 (2013).
- 26 Dikin, D. A. *et al.* Coexistence of superconductivity and ferromagnetism in two dimensions. *Phys Rev Lett* **107**, 056802 (2011).
- 27 Ben Shalom, M., Sachs, M., Rakhmievitch, D., Palevski, A. & Dagan, Y. Tuning spin-orbit coupling and superconductivity at the SrTiO₃/LaAlO₃ interface: a magnetotransport study. *Phys Rev Lett* **104**, 126802 (2010).
- 28 Caviglia, A. D. *et al.* Tunable Rashba spin-orbit interaction at oxide interfaces. *Phys Rev Lett* **104**, 126803 (2010).
- 29 Wang, H., Chan, C. H., Suen, C. H., Lau, S. P. & Dai, J. Y. Magnetotransport Properties of Layered Topological Material ZrTe₂ Thin Film. *ACS Nano* **13**, 6008-6016 (2019).
- 30 Machado, A. J. S. *et al.* Evidence for topological behavior in superconducting Cu_xZrTe_{2-y}. *Physical Review B* **95**, 144505 (2017).
- 31 Kozuka, Y. *et al.* Two-dimensional normal-state quantum oscillations in a superconducting heterostructure. *Nature* **462**, 487-490 (2009).
- 32 Chen, Y. Z. *et al.* A high-mobility two-dimensional electron gas at the spinel/perovskite interface of γ-Al₂O₃/SrTiO₃. *Nat Commun* **4**, 1371 (2013).
- 33 Ben Shalom, M., Ron, A., Palevski, A. & Dagan, Y. Shubnikov-de Haas oscillations in SrTiO₃/LaAlO₃ interface. *Phys Rev Lett* **105**, 206401 (2010).
- 34 Yang, M. *et al.* High field magneto-transport in two-dimensional electron gas LaAlO₃/SrTiO₃. *Applied Physics Letters* **109** (2016).
- 35 McCollam, A. *et al.* Quantum oscillations and subband properties of the two-dimensional electron gas at the LaAlO₃/SrTiO₃ interface. *APL Materials* **2** (2014).
- 36 Rubi, K. *et al.* Aperiodic quantum oscillations in the two-dimensional electron gas at the LaAlO₃/SrTiO₃ interface. *npj Quantum Materials* **5** (2020).
- 37 Lin, X. *et al.* Critical Doping for the Onset of a Two-Band Superconducting Ground State in SrTiO_{3-δ}. *Physical Review Letters* **112** (2014).

- 38 Caviglia, A. D. *et al.* Two-dimensional quantum oscillations of the conductance at LaAlO₃/SrTiO₃ interfaces. *Phys Rev Lett* **105**, 236802 (2010).
- 39 Shimizu, S. *et al.* Giant thermoelectric power factor in ultrathin FeSe superconductor. *Nat. Commun.* **10**, 825 (2019).
- 40 Pallecchi, I. *et al.* Giant oscillating thermopower at oxide interfaces. *Nat Commun* **6**, 6678 (2015).
- 41 Wang, Q.-Y. *et al.* Interface-Induced High-Temperature Superconductivity in Single Unit-Cell FeSe Films on SrTiO₃. *Chinese Physics Letters* **29** (2012).
- 42 Zhang, W.-H. *et al.* Direct Observation of High-Temperature Superconductivity in One-Unit-Cell FeSe Films. *Chinese Physics Letters* **31** (2014).
- 43 Tang, C. *et al.* Interface-enhanced electron-phonon coupling and high-temperature superconductivity in potassium-coated ultrathin FeSe films on SrTiO₃. *Physical Review B* **93** (2016).
- 44 Song, C. L. *et al.* Observation of Double-Dome Superconductivity in Potassium-Doped FeSe Thin Films. *Phys Rev Lett* **116**, 157001 (2016).
- 45 Zhang, W. H. *et al.* Effects of Surface Electron Doping and Substrate on the Superconductivity of Epitaxial FeSe Films. *Nano Lett* **16**, 1969-1973 (2016).
- 46 Zhang, H. *et al.* Origin of charge transfer and enhanced electron-phonon coupling in single unit-cell FeSe films on SrTiO₃. *Nat Commun* **8**, 214 (2017).
- 47 Zhao, W. *et al.* Direct imaging of electron transfer and its influence on superconducting pairing at FeSe/SrTiO₃ interface. *Sci. Adv.* **4** (2018).
- 48 Wang, Q. *et al.* Thickness dependence of superconductivity and superconductor–insulator transition in ultrathin FeSe films on SrTiO₃ (001) substrate. *2D Materials* **2** (2015).
- 49 Fletcher, R., Zaremba, E. & Zeitler, U. *Electron-Phonon Interactions in Low-Dimensional Structures*. Chap. 5 (Oxford University Press, 2003).
- 50 Gallagher, B. L. & Bucher, P. N. *Handbook on Semiconductors*. Vol. 1 817 (Elsevier, 1992).
- 51 Wang, G., Endicott, L., Chi, H., Lost'ak, P. & Uher, C. Tuning the temperature domain of phonon drag in thin films by the choice of substrate. *Phys. Rev. Lett.* **111**, 046803 (2013).
- 52 Martelli, V., Jimenez, J. L., Continentino, M., Baggio-Saitovitch, E. & Behnia, K. Thermal transport and phonon hydrodynamics in strontium titanate. *Phys. Rev. Lett.* **120** (2018).
- 53 Valentina, M., Julio, L. J., Mucio, C., Elisa, B. S. & B., K. Thermal transport and phonon hydrodynamics in strontium titanate. *Phys Rev Lett* **120**, 125901 (2018).
- 54 Wei, J. *et al.* Review of current high-ZT thermoelectric materials. *Journal of Materials Science* **55**, 12642-12704 (2020).

Figures

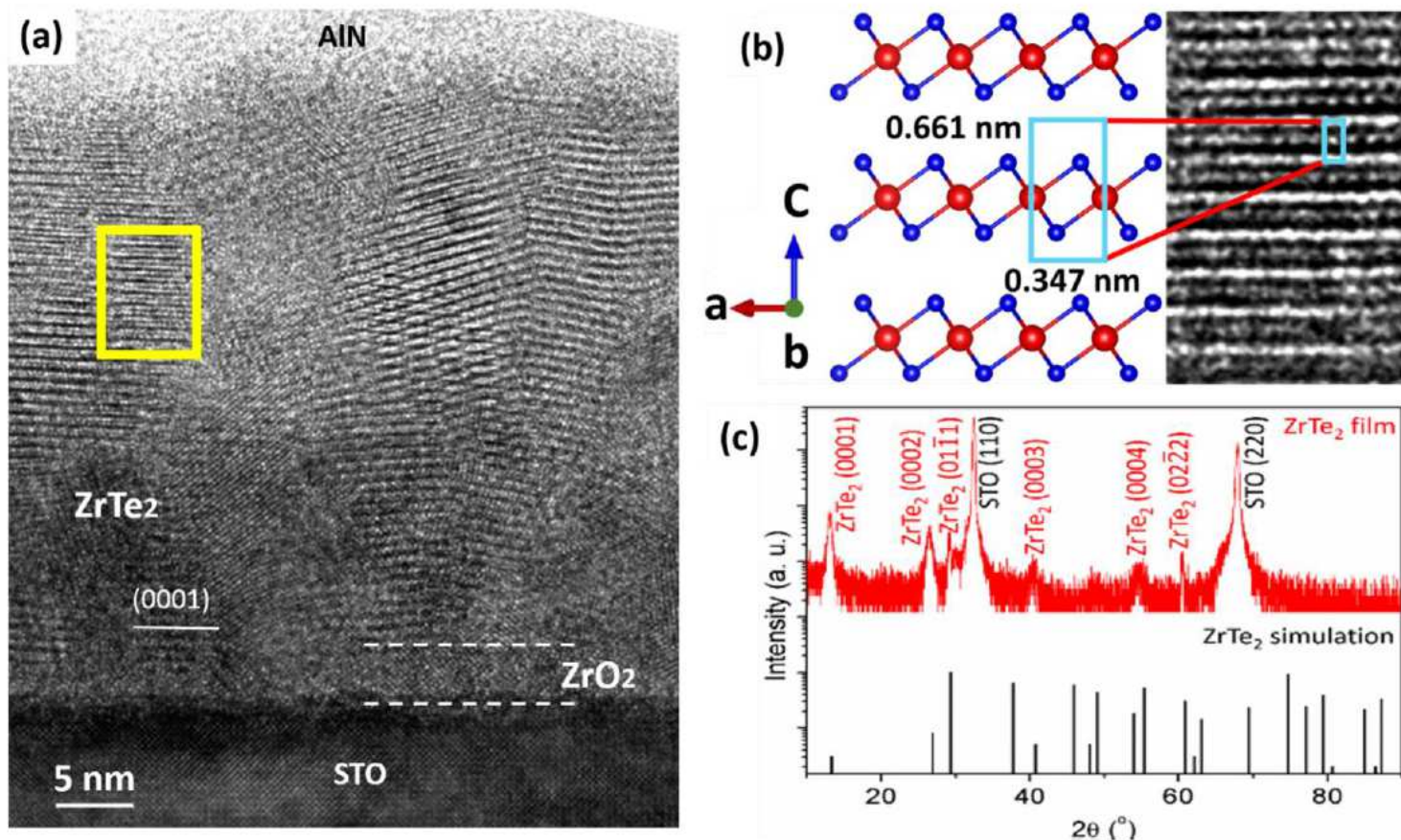


Figure 1

Crystal structure characterizations. (a) High-resolution TEM image of the ZrTe₂ film on STO substrate, where an interfacial layer of ZrO₂ reaction phase can be identified between the STO substrate and the ZrTe₂ film. (b) Magnified image of yellow rectangle region in (a) showing the correspondence of real unit cell with the crystal structure model of ZrTe₂. The unit cell is denoted by a rectangle to compared with magnified high-resolution TEM image of the ZrTe₂ film. (c) Typical XRD patterns of 60 nm ZrTe₂ film. The ZrTe₂ simulation pattern (JCPDS #54-560) is also illustrated for comparison.

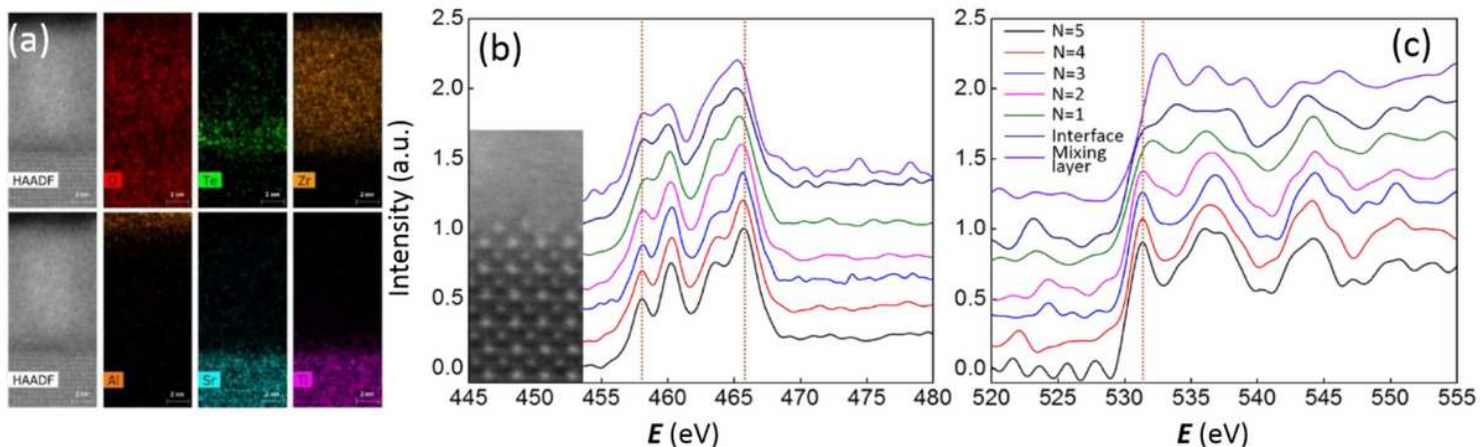


Figure 2

Elemental mapping and interfacial valence states of Ti and O ions (a) STEM-EDS element mapping across the interface, (b) EELS results of Ti-3d L edge shift peaks, and (c) O-2p K edge fine structure across the interface.

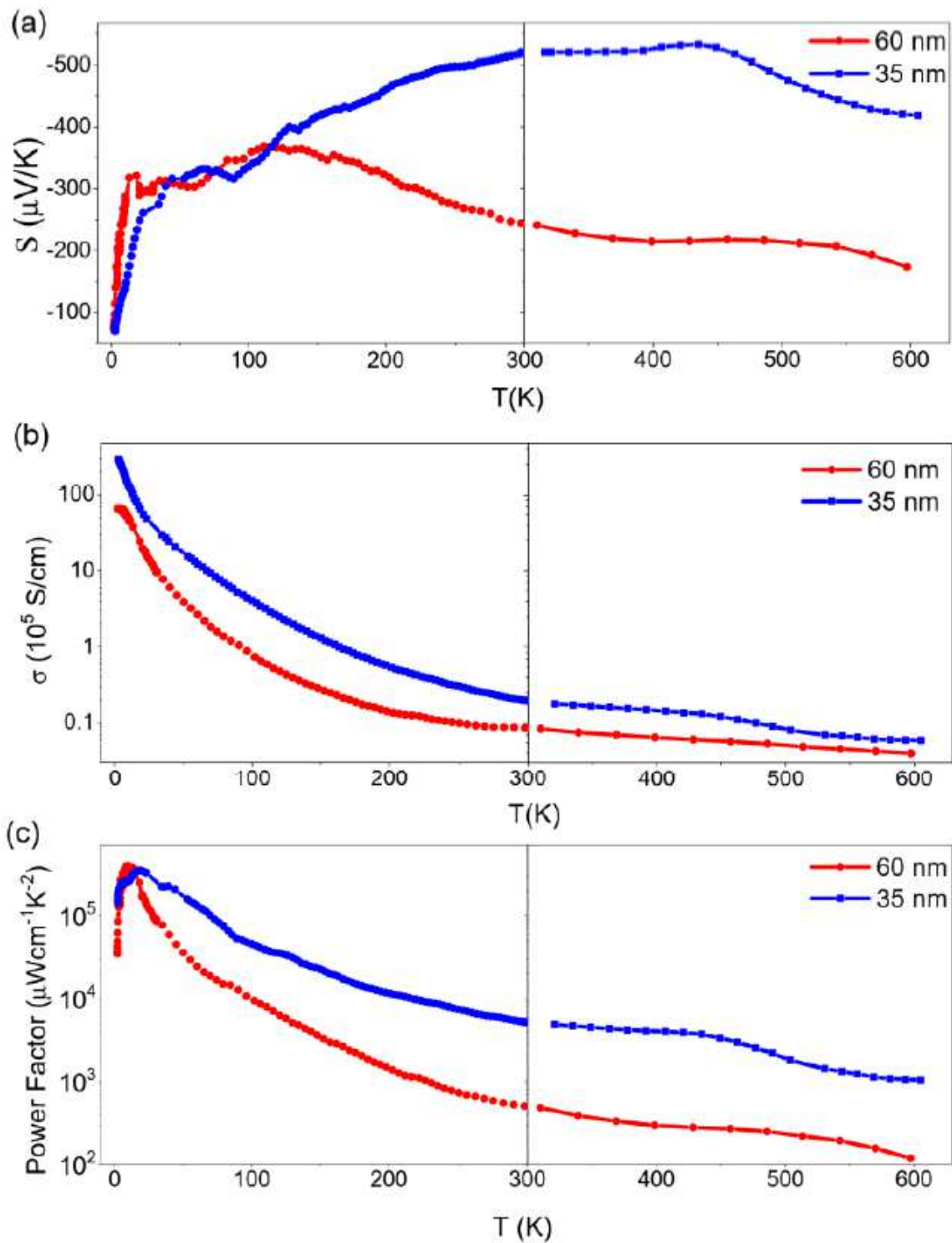


Figure 3

Thermoelectric and electrical conductive properties. (a) Seebeck coefficients, (b) electrical conductivities, and (c) thermoelectric power factors, of the ZrTe₂/STO heterostructures with 35 nm and 60 nm-thick ZrTe₂ films.

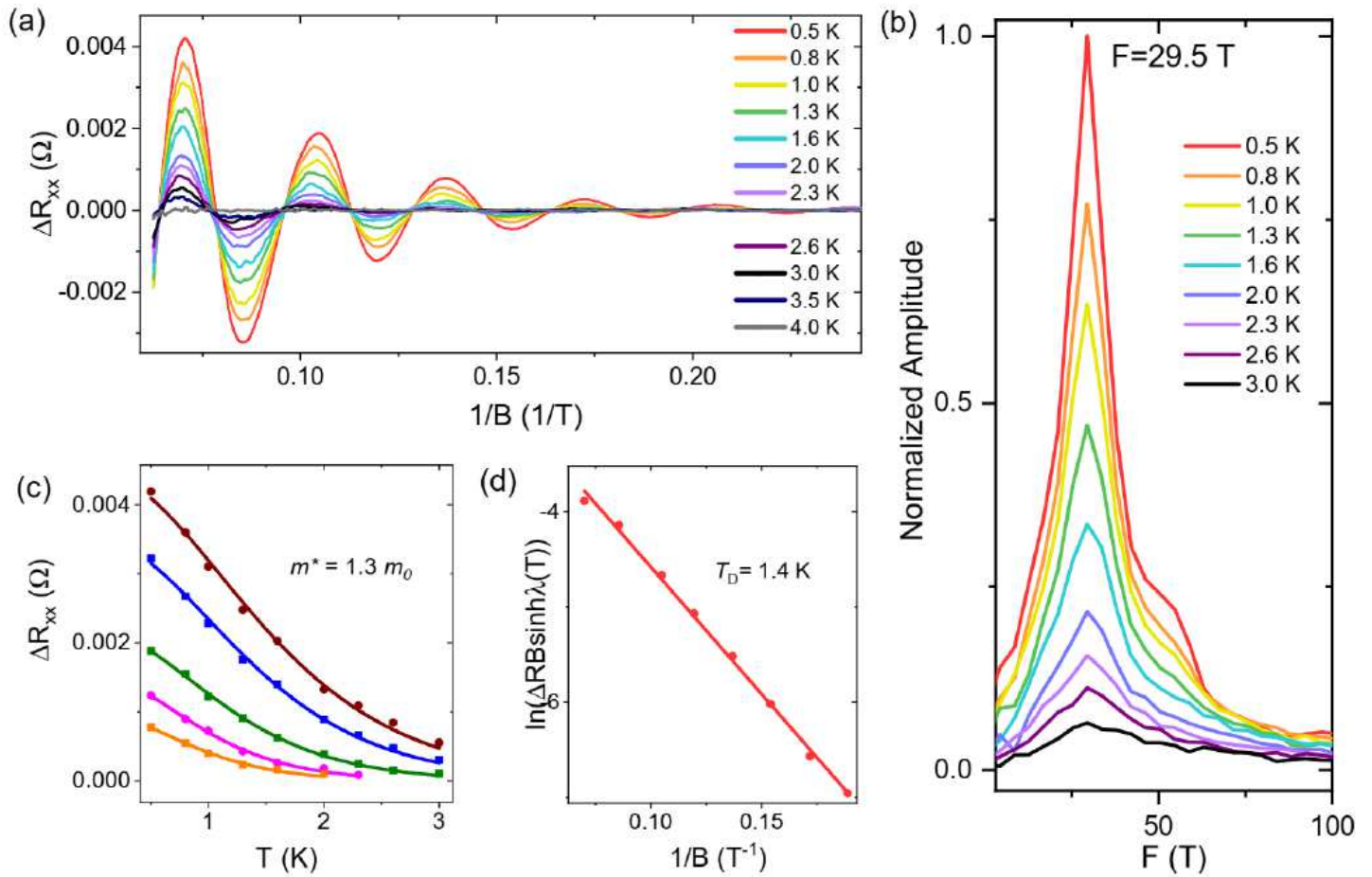


Figure 4

Quasi two-dimensional transport characteristics of the heterostructure. (a) SdH quantum oscillations in the ZrTe₂/STO, and (b) FFT results of the oscillations revealing a frequency peak of 29.5 T. (c) and (d) are calculated effective mass and Dingle temperature based on the Lifshitz-Kosevich formula.